



## Article

# Magnetic Field Effect on Sisko Fluid Flow Containing Gold Nanoparticles through a Porous Curved Surface in the Presence of Radiation and Partial Slip

Umair Khan <sup>1,2</sup> , Aurang Zaib <sup>3</sup> and Anuar Ishak <sup>1,\*</sup> 

<sup>1</sup> Department of Mathematical Sciences, Faculty of Science and Technology, Universiti Kebangsaan Malaysia, UKM Bangi 43600, Malaysia; umairkhan@iba-suk.edu.pk

<sup>2</sup> Department of Mathematics and Social Sciences, Sukkur IBA University, Sukkur 65200, Pakistan

<sup>3</sup> Department of Mathematical Sciences, Federal Urdu University of Arts, Science & Technology, Gulshan-e-Iqbal Karachi 75300, Pakistan; aurangzaib@fuuast.edu.pk

\* Correspondence: anuar\_mi@ukm.edu.my

**Abstract:** The radiation and magnetic field effects of nanofluids play a significant role in biomedical engineering and medical treatment. This study investigated the performance of gold particles in blood flow (Sisko fluid flow) over a porous, slippery, curved surface. The partial slip effect was considered to examine the characteristics of nanofluid flow in depth. The foremost partial differential equations of the Sisko model were reduced to ordinary differential equations by using suitable variables, and the boundary value problem of the fourth-order (bvp4c) procedure was applied to plot the results. In addition, the effects of the parameters involved on temperature and velocity were presented in light of the parametric investigation. A comparison with published results showed excellent agreement. The velocity distribution was enhanced due to the magnetic field, while the temperature increased due to the effects of a magnetic field and radiation, which are effective in therapeutic hyperthermia. In addition, the nanoparticle suspension showed increased temperature and decelerated velocity.

**Keywords:** Sisko fluid flow; gold particles; magnetohydrodynamics (MHD); radiation effect; slip effect; curved surface



**Citation:** Khan, U.; Zaib, A.; Ishak, A. Magnetic Field Effect on Sisko Fluid Flow Containing Gold Nanoparticles through a Porous Curved Surface in the Presence of Radiation and Partial Slip. *Mathematics* **2021**, *9*, 921. <https://doi.org/10.3390/math9090921>

Academic Editor: Mostafa Safdari Shadloo

Received: 27 January 2021

Accepted: 19 April 2021

Published: 21 April 2021

**Publisher's Note:** MDPI stays neutral with regard to jurisdictional claims in published maps and institutional affiliations.



**Copyright:** © 2021 by the authors. Licensee MDPI, Basel, Switzerland. This article is an open access article distributed under the terms and conditions of the Creative Commons Attribution (CC BY) license (<https://creativecommons.org/licenses/by/4.0/>).

## 1. Introduction

Nanofluids are a prominent topic of research. They have a wide range of applications in engineering and technology fields. Nanofluids have potential benefits in cancer therapy, drug delivery, nuclear reactors, and solar energy. Growth enrichment and convection thermal conductivity are needed during fluid flow when an outside source is essential. Nanofluids are synthesized by scattering nanoparticles in regular fluids. In addition to regular fluids, such as lubricant, oils, water, and polymer solutions, biological fluids can also be used as base fluids. A notable development in this area was investigated after the initial research by Choi [1]. Eastman et al. [2] experimentally analyzed heat transport in the presence of water-based CuO particles and ethylene-glycol-based Al<sub>2</sub>O<sub>3</sub> particles. Since then, different researchers have discussed the features of nanofluids [3–12]. However, the use of gold nanoparticles (Au-NPs) in biomedical science is also important, and Au-NPs can be used as therapeutic agents. They are currently used as contrast and photovoltaic agents and as drug transporters. In addition, Au-NPs have many characteristics that make them suitable for use in cancer treatment. Furthermore, owing to the high atomic number of gold, Au-NPs engender heat, which can be used for photothermal therapy of tumorous glands [13,14].

Non-Newtonian fluids play an imperative role in numerous manufacturing and engineering processes, such as food processing, petroleum digging, and chemical and

biological treatment. Previously, blood was treated as a Newtonian fluid [15]; however, Thurston [16] clarified that visco-elasticity is considered a basic property of rheological blood, which indicates that human blood is non-Newtonian, depending on the visco-elastic performance of red blood cells. Several non-Newtonian fluids are treated as blood, e.g., Sisko fluid. Khan and Shahzad [17] inspected Sisko fluid flow over a stretching sheet. Munir et al. [18] extended this research by considering the bidirectional Sisko fluid flow over a stretching surface. Khan et al. explored the effects of a magnetic field and radiation on Sisko fluid flow over a bidirectional stretching sheet [19]. Eid et al. [20] used gold nanoparticles to investigate the effects of radiation on Sisko biofluid flow over a nonlinear stretching sheet. Ahmad et al. [21] numerically investigated the significance of Sisko fluid flow over a stretching curved sheet using a nanofluid and a magnetic field. Khan et al. [22] investigated 2D Sisko fluid flow impeding nanoparticles via a radially stretching/shrinking sheet under zero-flux conditions.

The effect of radiation on blood flow is considered important in biomedical science and other medical treatment techniques, especially in thermal therapeutic procedures. One effective technique commonly used for heat treatment of different body parts is infrared radiation. This method is favored in heat therapy because it is applied directly to blood capillaries in the affected regions. In addition, it is used in the treatment of bursitis, which is inflammation of the fluid-filled sacs (bursae) that lie between bone and tendon or between skin and tendon. Inoue and Kabaya [23], Kobu [24], and Nishimoto et al. [25] experimentally investigated the effects of infrared radiation on blood flow. He et al. [26] used laser irradiation to analyze oxygen transport, temperature, and blood flow in breast tumors. Prakash and Makinde [27] explored the effects of radiation on blood flow with heat transport through an artery with stenosis. Misra and Sinha investigated the effects of a magnetic field and radiation on time-dependent blood flows with heat transfer through a porous capillary in a stretching motion [28]. Khan et al. [29] used gold nanoparticles to investigate the effects of a magnetic field on radiative blood flow over a slippery surface and obtained multiple solutions. In addition, Zaib et al. investigated the effects of a magnetic field and radiation on the mixed convective flow of a tangent hyperbolic fluid over a flat, non-isothermal vertical plate [30].

The present study investigated radiative blood flow with heat transport using a Sisko fluid containing gold nanoparticles, over a porous, curved surface with a magnetic field and partial slip. The governing partial differential equations were converted to a system of ordinary differential equations before they were solved numerically via the boundary value problem of the fourth-order (bvp4c) function available in MATLAB software, which is based on the Lobatto IIIA technique. To analyze the capability of the numerical solution process, the skin friction coefficient was compared with published results. Graphical results were presented for the velocity profile, temperature distribution, skin friction, and heat transfer rate for different values of the parameters involved. To the best of our knowledge, no study has investigated flow situations with gold nanoparticles using the Sisko model with similarity solutions. The results have implications for clinical sciences, especially in thermal therapy.

## 2. Problem Definition and Modeling

### 2.1. Problem Definition

The steady flow of a non-Newtonian fluid containing gold nanoparticles over a porous curved surface was examined. According to Chen [31], blood is treated as an electric conducting fluid. Thus, blood flow in nature is magnetohydrodynamic. Blood flow is due to the movement of the stretching surface along the  $s$  direction and suction along the  $r$  direction. In addition, the stretching curve is coiled in a circle of radius  $R$  and center  $O$  and contains 12–85 nm gold nanoparticles, as shown in Figure 1. A magnetic field  $B_0$  is applied normal to the curved surface. A larger  $R$  signifies a vaguely curved surface. Moreover, the stretching and shrinking sheet of the curved surface depends upon the arbitrary constant ( $c > 0$  for stretching and  $c < 0$  for shrinking), where velocity is represented as  $U_w(s) = cs$ ,

with  $c > 0$ , which moves along the  $s$  direction, and suction velocity is represented as  $v_0$ . In addition, the characteristics of nanoparticles and the carrier-based fluid are assumed to be constant. The temperature and ambient temperature of the surface are represented, respectively, as  $T_w$  and  $T_\infty$ . The radiation and partial slip effects are also incorporated.

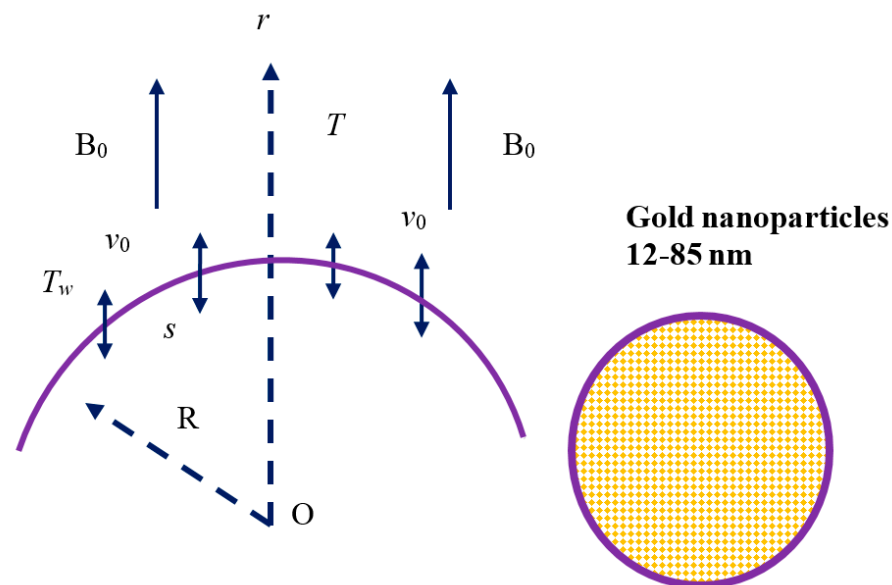


Figure 1. Physical diagram of the problem.

## 2.2. Flow Analysis

Using boundary layer approximations, the governing equations involving the magnetic effect on Sisko blood flow with gold nanoparticles over a porous, curved surface with radiation and partial slip are

$$\frac{\partial}{\partial r}[(r+R)v] + R \frac{\partial u}{\partial s} = 0, \quad (1)$$

$$\frac{1}{(r+R)} u^2 = \frac{1}{\rho_{nf}} \frac{\partial p}{\partial r}, \quad (2)$$

$$v \frac{\partial u}{\partial r} + \frac{b}{\rho_{nf}(r+R)^2} \frac{\partial}{\partial r} \left[ (r+R)^2 \left( -\left( \frac{\partial u}{\partial r} - \frac{u}{r+R} \right) \right)^n \right] + \left( \frac{Ru}{r+R} \right) \frac{\partial u}{\partial s} + \frac{uv}{(r+R)} = -\frac{1}{\rho_{nf}} \left( \frac{R}{r+R} \right) \frac{\partial p}{\partial s} - \frac{\sigma_{nf} B_0^2}{\rho_{nf}} u + \frac{\mu_{nf}}{\rho_{nf}(r+R)^2} \frac{\partial}{\partial r} \left[ (r+R)^2 \left( \frac{\partial u}{\partial r} - \frac{u}{r+R} \right) \right], \quad (3)$$

$$v \frac{\partial T}{\partial r} + \frac{1}{(c_p \rho)_{nf}(r+R)} \frac{\partial}{\partial r} [(r+R)q_r^*] + \left( \frac{Ru}{r+R} \right) \frac{\partial T}{\partial s} = \frac{k_{nf}}{(c_p \rho)_{nf}} \left( \frac{\partial^2 T}{\partial r^2} + \frac{1}{(r+R)} \frac{\partial T}{\partial r} \right), \quad (4)$$

with the boundary conditions

$$\begin{cases} u = \lambda U_w + L \left[ \frac{\partial u}{\partial r} - \frac{u}{r+R} \right], v = v_0, T = T_w \text{ at } r = 0, \\ u \rightarrow 0, \frac{\partial u}{\partial r} \rightarrow 0, T \rightarrow T_\infty \text{ as } r \rightarrow \infty. \end{cases} \quad (5)$$

Here,  $u$  and  $v$  are components of the velocity, such that the corresponding stretching velocity moves along the axial  $s$  direction and suction along the radial  $r$  direction, respectively. In addition,  $n$  and  $b$  are material constants,  $L$  constant slip parameter,  $p$  the pressure,  $R$  the radius of curvature, and  $T$  the nanofluid temperature. In Equation (4), the relative heat flux is represented by  $q_r^*$  and can be articulated by employing the Rosseland approximation as

$$q_r^* = -4(3k_1)^{-1} \sigma_1 \frac{\partial T^4}{\partial r}, \quad (6)$$

where  $\sigma_1$  is the mean proportion coefficient and  $k_1$  the Stefan–Boltzmann constant. Thus, the term  $T^4$  at point  $T_\infty$  is exercised by the Taylor series. Avoiding the highest-order terms, we get

$$T^4 \approx 4TT_\infty^3 - 3T_\infty^4 \quad (7)$$

The thermo-physical quantities of the gold particle nanofluid introduced in the governing equations are given by

$$\begin{aligned} \frac{\mu_{nf}}{\mu_f} &= 1 + 7.3\phi + 123\phi^2 \quad \text{for } \phi > 0.02, \quad \frac{\rho_{nf}}{\rho_f} = (1 - \phi) + \frac{\rho_{s1}}{\rho_f}\phi, \\ \frac{(c_p\rho)_{nf}}{(c_p\rho)_f} &= (1 - \phi) + \frac{(c_p\rho)_{s1}}{(c_p\rho)_f}\phi, \quad \frac{k_{nf}}{k_f} = \left[ \frac{(k_{s1} + 2k_f) - 2(\phi k_f - \phi k_{s1})}{(k_{s1} + 2k_f) + \phi(k_f - k_{s1})} \right], \\ \frac{\sigma_{nf}}{\sigma_f} &= \left( 1 + \frac{3\phi \left( \frac{\sigma_{s1}}{\sigma_f} - 1 \right)}{\left( \frac{\sigma_{s1}}{\sigma_f} + 2 \right) - \left( \frac{\sigma_{s1}}{\sigma_f} - 1 \right)\phi} \right), \end{aligned} \quad (8)$$

where  $k_f, \rho_f, \mu_f$  and  $\sigma_f$  are the thermal conductivity, density, viscosity, and electrical conductivity of the carrier-based fluid, respectively;  $k_{nf}, \rho_{nf}, \mu_{nf}$  and  $\sigma_{nf}$  are the corresponding quantities of the nanofluid, respectively;  $c_p$  is the heat capacity; and subscripts  $f, nf$ , and  $s_1$  are quantities of the carrier-based fluid, the nanofluid, and the solid volume fraction of the nanoparticles, respectively.

Upon applying the following similarity transformation:

$$\begin{aligned} u &= csF'(\eta), \quad v = \frac{-csR}{r+R} \text{Re}_b^{-\frac{1}{n+1}} \frac{1}{n+1} [2nF(\eta) + (1-n)\eta F'(\eta)], \\ \psi &= cs^2 \text{Re}_b^{-\frac{1}{n+1}} F(\eta), \quad \eta = \left( \frac{r}{s} \right) \text{Re}_b^{\frac{1}{n+1}}, \quad p = \rho_f c^2 s^2 P(\eta), \quad \theta(\eta) = \frac{T - T_\infty}{T_w - T_\infty}. \end{aligned} \quad (9)$$

Equation (1) is satisfied identically, whereas Equations (2)–(5) become

$$\frac{\partial P}{\partial \eta} = \frac{F'^2}{\eta + B} \quad (10)$$

$$\begin{aligned} \frac{2BP}{(\eta+B)\frac{\rho_{nf}}{\rho_f}} &= \frac{B}{\eta+B} \left( \frac{2n}{n+1} \right) \left( FF'' + \frac{FF'}{\eta+B} \right) - \frac{B}{\eta+B} F'^2 + \frac{\mu_{nf}}{\rho_{nf}} B_1 \left( F''' \frac{F'}{(\eta+B)^2} + \frac{F''}{\eta+B} \right) + \\ &\frac{n}{\rho_{nf}} \left( - \left( F'' \frac{F'}{\eta+B} \right) \right)^{n-1} \left( F''' + \frac{F'}{(\eta+B)^2} - \frac{F''}{\eta+B} \right) - \frac{2}{(\eta+B)\frac{\rho_{nf}}{\rho_f}} \left( - \left( F'' \frac{F'}{\eta+B} \right) \right)^n - M \frac{\sigma_{nf}}{\rho_{nf}} F', \end{aligned} \quad (11)$$

By removing the pressure term from Equations (10) and (11), we obtain the following equations, along with the dimensionless form of the energy equation:

$$\begin{aligned} \frac{\Sigma_1}{\Sigma_2} B_1 \left( F'''' + \frac{2F'''}{\eta+B} + \frac{F'}{(\eta+B)^3} - \frac{F''}{(\eta+B)^2} \right) &+ \left( \frac{2n}{n+1} \right) \left[ \left( \frac{B}{\eta+B} \right) (FF''' + F'F'') + \left( \frac{B}{(\eta+B)^2} \right) (FF'' + F'^2) - \frac{BFF'}{(\eta+B)^3} \right] \\ &- \frac{2BF'F''}{\eta+B} - \frac{2BF'^2}{(\eta+B)^2} + \frac{n}{\Sigma_2} \left( - \left( F'' \frac{F'}{\eta+B} \right) \right)^{n-1} \left( F''' + \frac{2F'''}{\eta+B} - \frac{F''}{(\eta+B)^2} \right) \\ &+ \frac{F'}{(\eta+B)^3} \left( F''' + \frac{2F'''}{\eta+B} - \frac{F''}{(\eta+B)^2} \right) - \frac{n(n-1)}{\Sigma_2} \left( - \left( F'' \frac{F'}{\eta+B} \right) \right)^{n-2} \left( F''' + \frac{F'}{(\eta+B)^2} - \frac{F''}{\eta+B} \right)^2 \\ &- \frac{\Sigma_3}{\Sigma_2} M \left( \frac{F'}{\eta+B} + F'' \right) = 0, \end{aligned} \quad (12)$$

$$\left( \Sigma_4 + \frac{4}{3} R_d \right) \left( \theta'' + \frac{\theta'}{\eta+B} \right) + \text{Pr} \Sigma_5 \frac{B}{\eta+B} \left( \frac{2n}{n+1} \right) F\theta' = 0, \quad (13)$$

in which:

$$\frac{\mu_{nf}}{\mu_f} = \Sigma_1, \frac{\rho_{nf}}{\rho_f} = \Sigma_2, \frac{\sigma_{nf}}{\sigma_f} = \Sigma_3, \frac{k_{nf}}{k_f} = \Sigma_4, \frac{(\rho c_p)_{nf}}{(\rho c_p)_f} = \Sigma_5.$$

### 2.3. Outcome of the Parameterization

The physical parameters in Equations (12) and (13) are radiation  $R_d$ ; the Prandtl number  $Pr$ ; the local Reynolds numbers  $Re_s$  and  $Re_b$ ; the material parameter of the Sisko fluid,  $B_1$ ; the magnetic parameter  $M$ ; the radius of curvature  $B$ ; the thermal conductivity  $\alpha_f$ ; the slip parameter  $B_2$ ; and the suction parameter  $S$ , which are obtained as follows:

$$R_d = \frac{4\sigma_1 T_\infty^3}{k_1 k_f}, Pr = \frac{\mu_w}{\alpha_f} Re_b^{\frac{-2}{n+1}}, Re_s = \frac{u_w s}{\nu_f}, Re_b = \frac{u_w^{2-n} s^n \rho_f}{b}, B_1 = \frac{Re_b^{\frac{2}{n+1}}}{Re_s}, M = \frac{\sigma_f B_0^2}{\rho_f c}, \\ B = \frac{R}{s} Re_b^{\frac{1}{n+1}}, \alpha_f = \frac{k_f}{(c_p \rho)_f}, B_2 = \frac{L}{s} Re_b^{\frac{1}{n+1}}, S = \frac{-v_0}{u_w} \left( \frac{n+1}{2n} \right) Re_b^{\frac{1}{n+1}}.$$

The boundary conditions are

$$\begin{cases} F'(0) = \lambda + B_2 \left( F''(0) - \frac{F'(0)}{B} \right), F(0) = S, \theta(0) = 1 \text{ at } \eta = 0, \\ F'(\infty) \rightarrow 0, F''(\infty) \rightarrow 0, \theta(\infty) \rightarrow 0 \text{ as } \eta \rightarrow \infty. \end{cases} \quad (14)$$

The pressure term can be obtained from Equation (11), which becomes:

$$P = \frac{(\eta + B) \frac{\rho_{nf}}{\rho_f}}{2B} \left[ \begin{aligned} & \frac{B}{\eta + B} \left( \frac{2n}{n+1} \right) \left( FF'' + \frac{FF'}{\eta + B} \right) - \frac{B}{\eta + B} F'^2 + \frac{\mu_{nf}}{\rho_{nf}} B_1 \left( \frac{F'''}{(\eta + B)^2} + \frac{F''}{\eta + B} \right) + \\ & \frac{n}{\frac{\rho_{nf}}{\rho_f}} \left( - \left( F'' - \frac{F'}{\eta + B} \right) \right)^{n-1} \left( F''' - \frac{F''}{\eta + B} + \frac{F'}{(\eta + B)^2} \right) - \\ & \frac{2}{(\eta + B) \frac{\rho_{nf}}{\rho_f}} \left( - \left( F'' - \frac{F'}{\eta + B} \right) \right)^n - M \frac{\sigma_{nf}}{\rho_{nf}} \frac{F'}{\rho_f} \end{aligned} \right] \quad (15)$$

### 2.4. Physical Parameters

Following an engineering approach, the quantities  $C_F$  (local skin friction coefficient) and  $Nu_s$  (Nusselt number) are expressed as follows:

$$C_F = \frac{2\tau_{rs}}{\rho_f u_w^2}, \quad (16)$$

where

$$\tau_{rs} = \mu_{nf} \left( \frac{\partial u}{\partial r} - \frac{u}{r + R} \right) - b \left[ - \left( \frac{\partial u}{\partial r} - \frac{u}{r + R} \right) \right]^n \Big|_{r=0}, \quad (17)$$

After transformation, the reduced skin friction coefficient becomes

$$\frac{1}{2} Re_b^{\frac{1}{n+1}} C_F = \Sigma_1 B_1 \left( F''(0) - \frac{F'(0)}{B} \right) - \left( - \left( F''(0) - \frac{F'(0)}{B} \right) \right)^n. \quad (18)$$

The heat transfer rate at the surface,  $Nu_s$  (Nusselt number), is

$$Nu_s = \frac{sq_w}{k_f (T_w - T_\infty)}, \quad (19)$$

where

$$q_w = -k_{nf} \left( \frac{\partial T}{\partial r} \right) \Big|_{r=0}. \quad (20)$$

After transformation, the reduced Nusselt number becomes

$$\text{Re}_b^{\frac{-1}{n+1}} Nu_s = -\Sigma_4 \theta'(0). \quad (21)$$

### 3. Results and Discussion

The nonlinear ordinary differential Equations (12) and (13) subject to boundary restrictions (Equation (14)) were solved numerically using the bvp4c function in the MATLAB software. The effects of various physical parameters (the magnetic parameter  $M$ , curvature parameter  $B$ , slip parameter  $B_2$ , nanoparticle volume fraction  $\phi$ , radiation parameter  $R_d$ , suction  $S$ , and stretching/shrinking parameter  $\lambda$ ) on the velocity profile, temperature distribution, skin friction coefficient, and heat transfer rate are illustrated in Figures 2–19 for both the carrier-based fluid ( $\phi = 0$ ) and the gold particle nanofluid ( $\phi = 0.035$ ). The parameters fixed throughout computation were  $B_1 = 1.1$ ,  $S = 3.5$ ,  $M = 0.5$ ,  $B_2 = 0.2$ ,  $\lambda = 1.5$ ,  $n = R_d = 2$ , and  $B = 1.5$ .

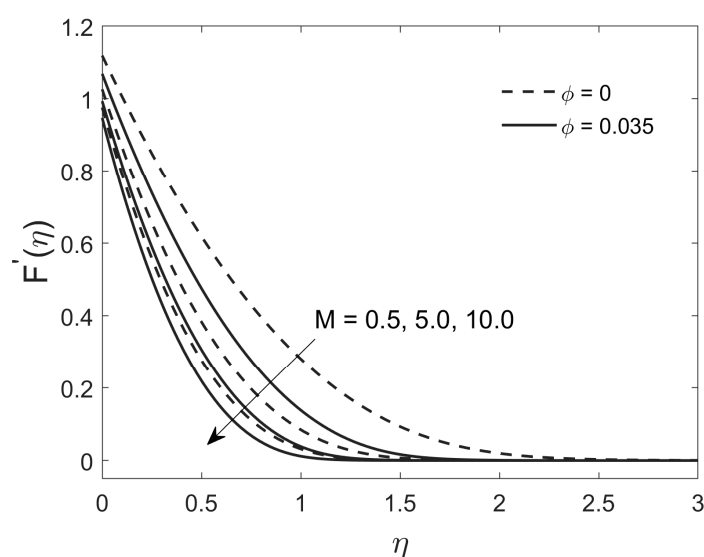


Figure 2. Effect of a magnetic field on the velocity profile.

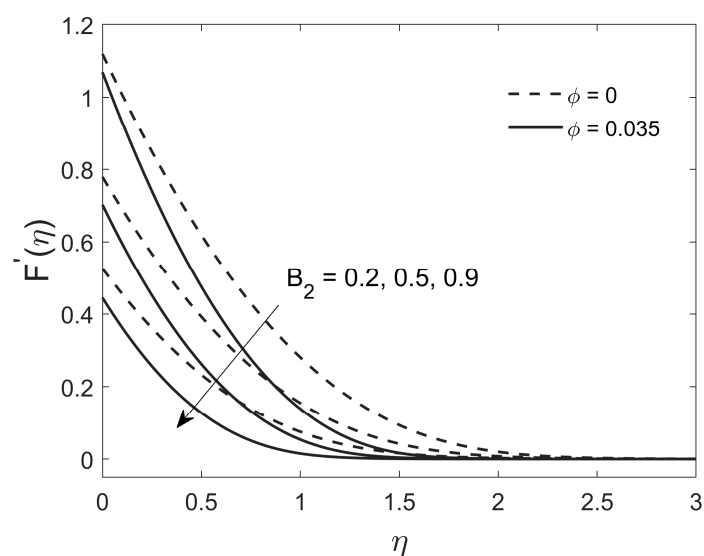


Figure 3. Effect of a partial slip on the velocity profile.

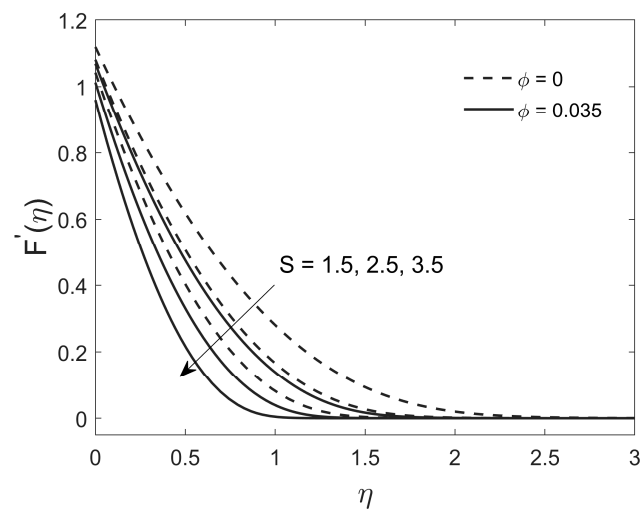


Figure 4. Effect of suction on the velocity profile.

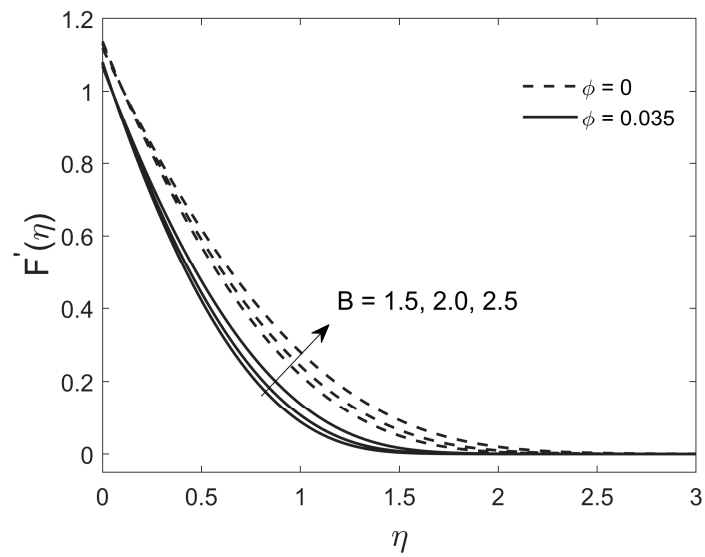


Figure 5. Effect of the radius of curvature on the velocity profile.

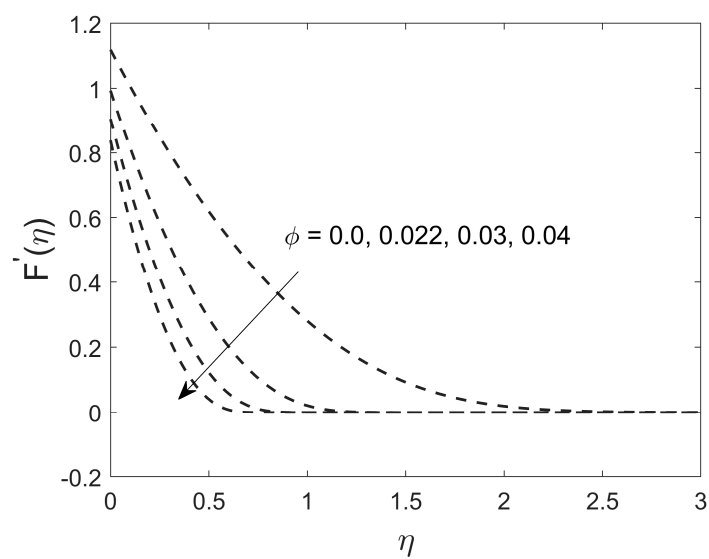


Figure 6. Effect of the nanoparticle volume fraction on the velocity profile.

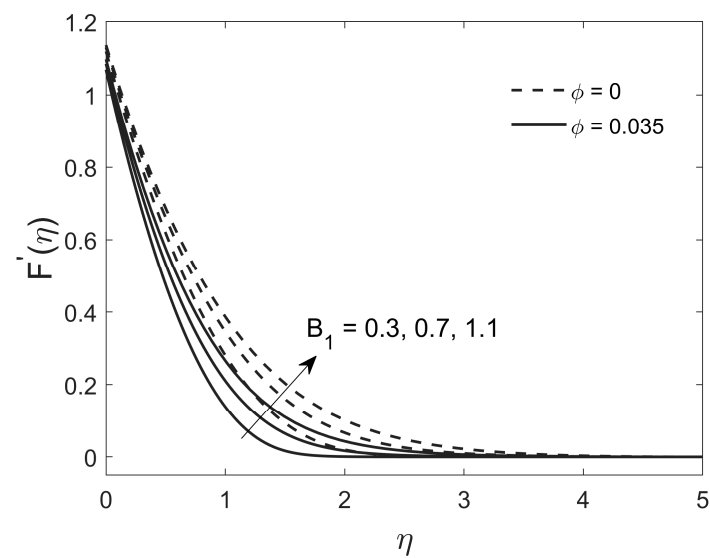


Figure 7. Effect of the material parameter on the velocity profile.

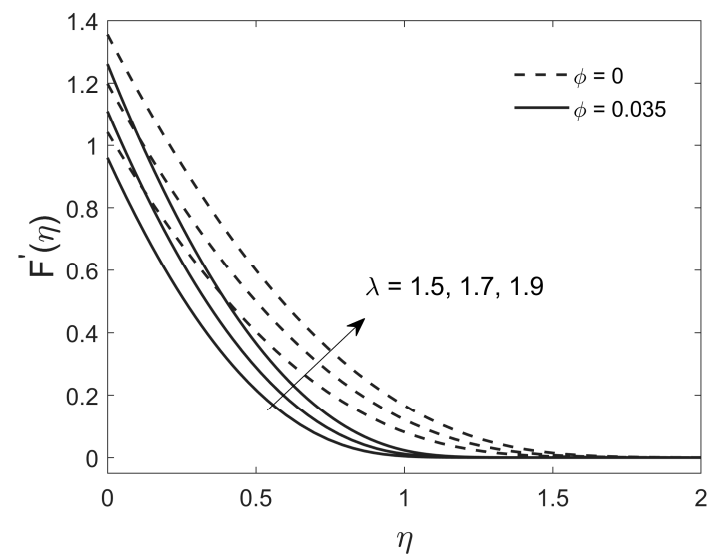


Figure 8. Effect of stretching/shrinking on the velocity profile.

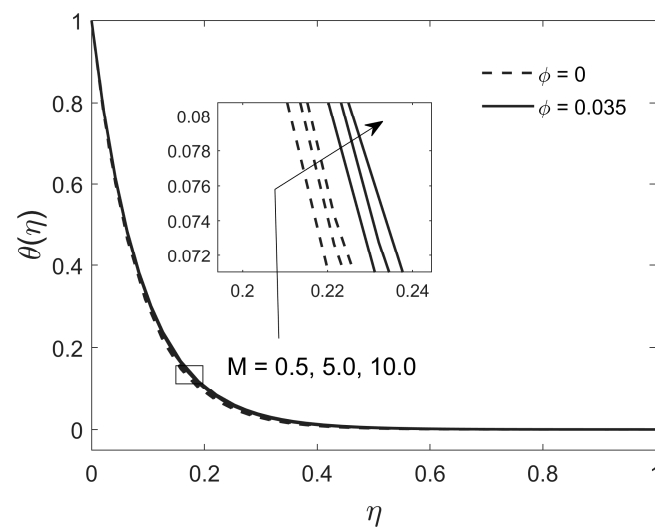


Figure 9. Effect of the magnetic field on the temperature distribution.



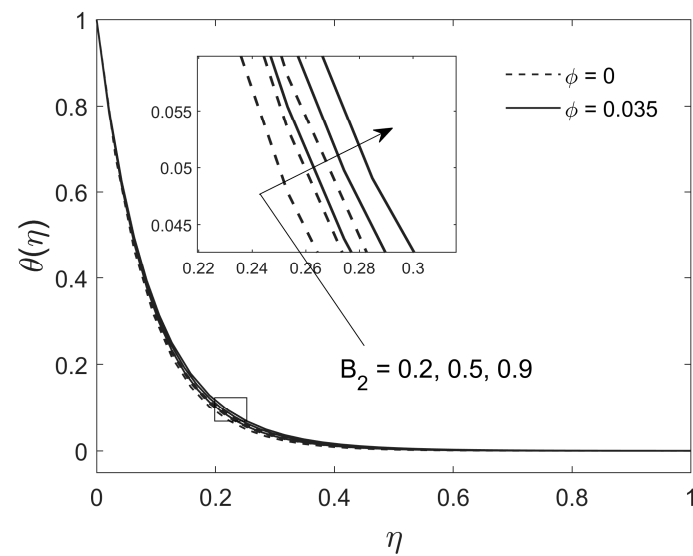


Figure 10. Effect of the slip on the temperature distribution.

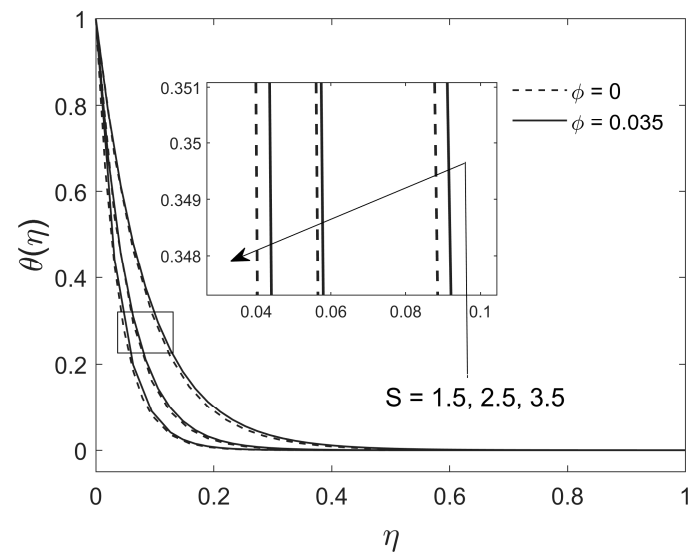


Figure 11. Effect of suction on the temperature distribution.

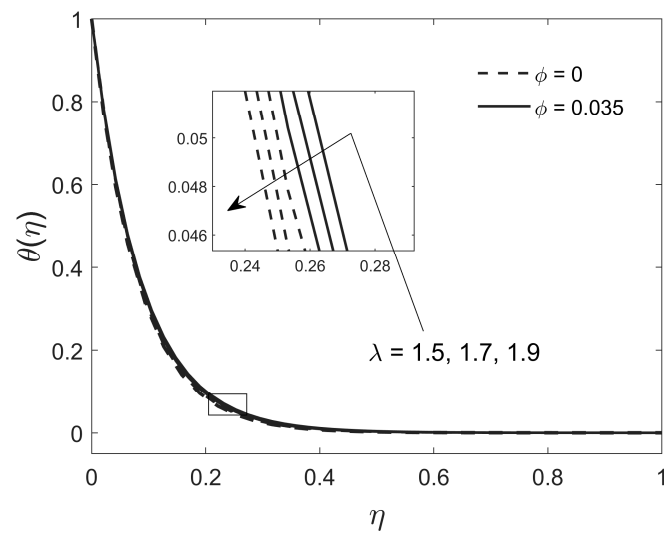


Figure 12. Effect of stretching/shrinking on the temperature distribution.

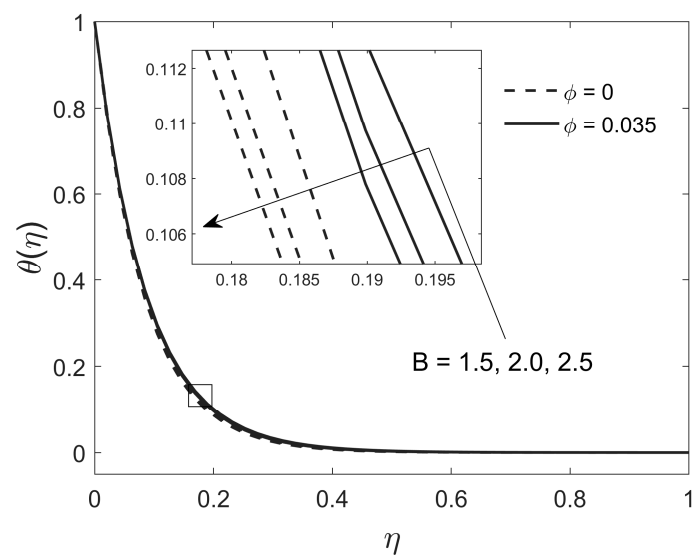


Figure 13. Effect of curvature on the temperature distribution.

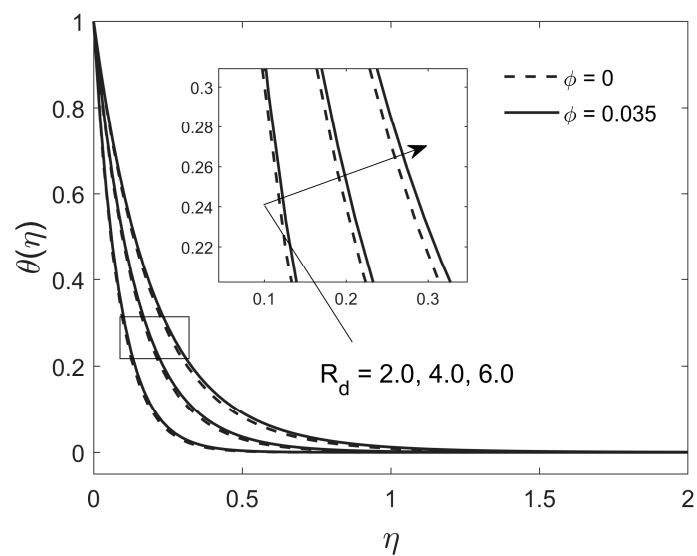


Figure 14. Effect of radiation on the temperature distribution.

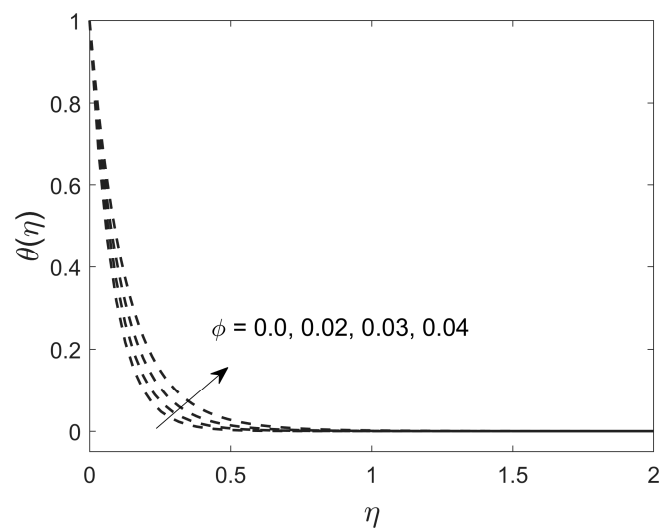


Figure 15. Effect of the nanoparticle volume fraction on the temperature distribution.

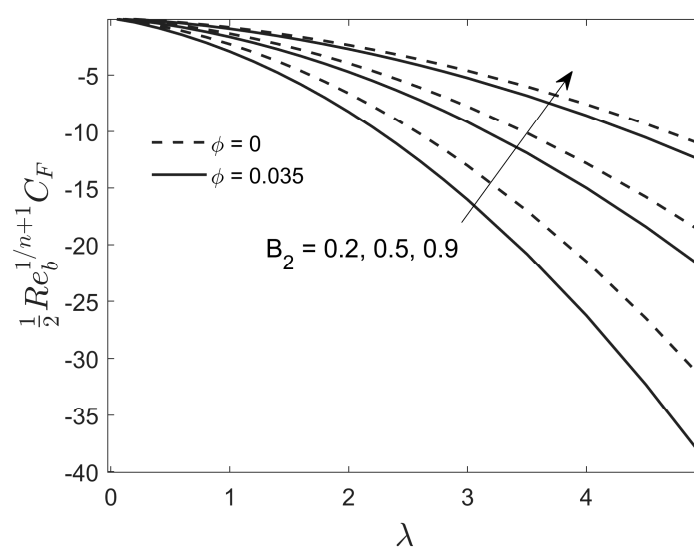


Figure 16. Effect of the slip on the skin friction coefficient against stretching/shrinking.

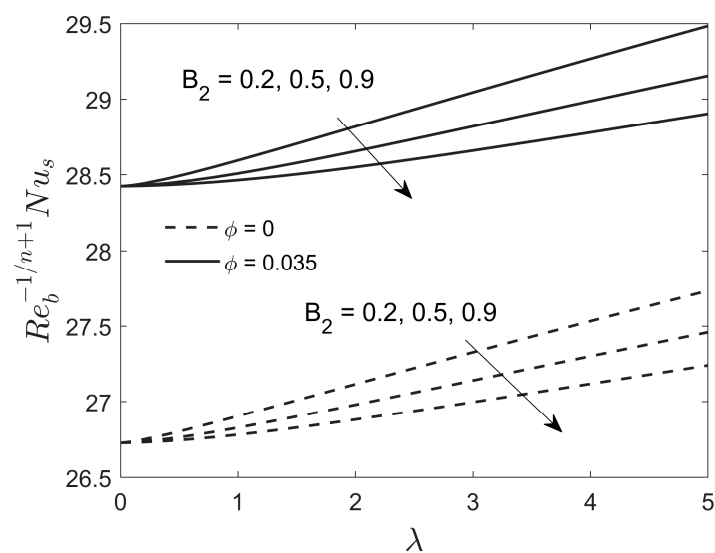


Figure 17. Effect of the slip on the Nusselt number against stretching/shrinking.

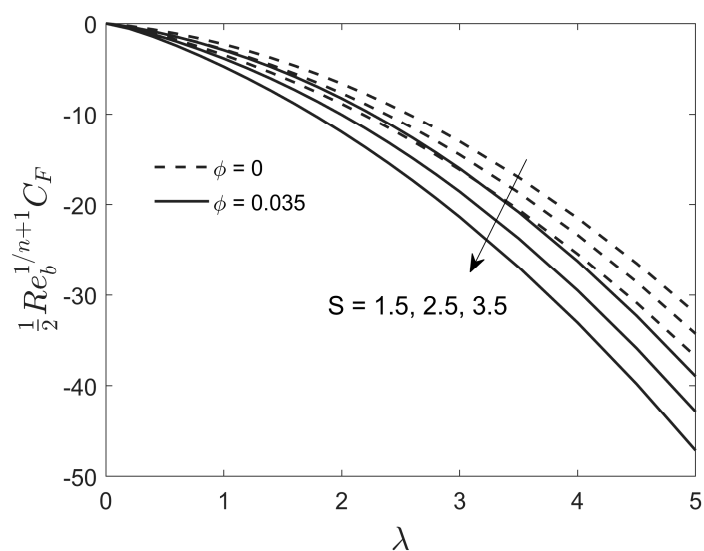
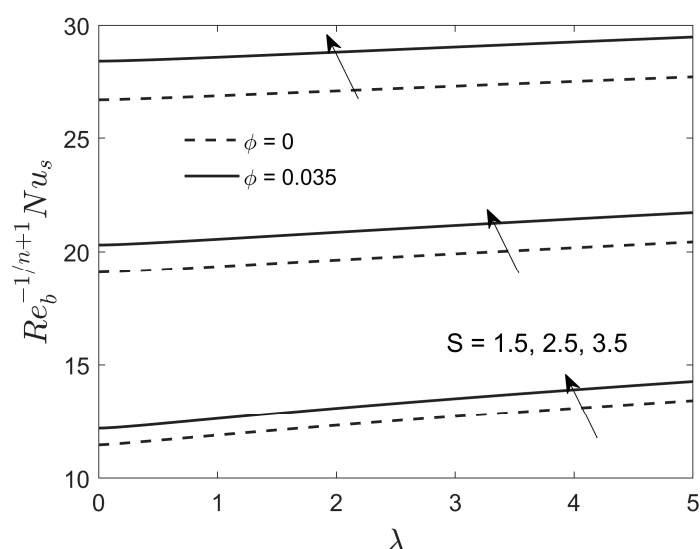


Figure 18. Effect of suction on the skin friction coefficient against stretching/shrinking.



**Figure 19.** Effect of suction on the Nusselt number against stretching/shrinking.

### 3.1. Effect of Physical Parameters on the Velocity Profile

Figures 2–6 demonstrate the behavior of the velocity profile at different values of  $M$ ,  $B_2$ ,  $S$ ,  $B$ , and nanoparticle volume fraction  $\phi$ . The velocity decreases due to the magnetic field for the carrier-based fluid and the gold particle nanofluid (Figure 2). Initially, the velocity and thickness of the momentum boundary layer for the carrier-based fluid are larger compared to those for the gold particle nanofluid. In addition, the velocity behavior of the gold particle nanofluid reduces more in the presence of gold nanoparticles, because gold nanoparticles generate friction in the fluid. Physically, increasing values of  $M$  augment the Lorentz force, which ultimately decreases velocity. Figure 2 also shows that the velocity of blood decreases. Figure 3 shows the effect of a partial slip on the velocity. The velocity of the fluid decreases for both the carrier-based fluid and the gold particle nanofluid. The velocity decreases in both fluids ( $\phi = 0$ ) and ( $\phi = 0.035$ ) with increasing  $B_2$ . The velocity reduction at the curve surface shows that the fluid flow occurs at the stretching curve surface; thus, any increase in the velocity slip parameter of the fluid at the stretching surface decreases the velocity field. Moreover, the higher values of  $B_2$  signify that the friction connecting the blood and the surface is removed. The impact of suction on the velocity is shown in Figure 4 for both the carrier-based fluid and the gold particle nanofluid. Physically, the resistance in the blood flow occurs because of viscosity, which can be handled by using suction. Increasing suction decreases the drag force at the sheet. Consequently, the momentum boundary layer thickness also reduces in both cases.

Figure 5 shows the effect of the curvature on the velocity profile, which increases the flow for both the carrier-based fluid and the gold particle nanofluid. The momentum boundary layer thickness and the magnitude of the velocity also improve with increasing curvature. Furthermore, the distance between the solution curves for the carrier-based fluid is slightly similar compared to that between the outcome curves of the gold particle nanofluid. Generally, this behavior of a fluid means that the bend of the curved stretching surface enhances fluid flow over it. This rise in the velocity gradient is slightly more in the carrier-based fluid compared to the gold particle nanofluid.

Figure 6 shows that the velocity of blood decreases as  $\phi$  increases, which is responsible for the reduction in the velocity of the boundary layer. Physically, a higher  $\phi$  enhances the blood viscosity, which consequently decreases the magnitude of the boundary layer thickness. Figures 7 and 8 show that the velocity increases for both the carrier-based fluid and the gold particle nanofluid due to the material and stretching/shrinking parameters. In addition, the magnitude of the velocity and the momentum boundary layer thickness increase with increasing material and stretching parameters. Both graphs are plotted for

both fluids, where the increase in velocity is more for the carrier-based fluid compared to the gold particle nanofluid.

### 3.2. Effect of Physical Parameters on the Temperature Distribution

Figures 9–15 show the effects of the magnetic, slip, suction, stretching/shrinking, curvature, and radiation parameters on the temperature for the carrier-based fluid and the gold particle nanofluid. Figure 9 shows that the temperature increases due to the magnetic field for both fluids. This is because inclusion of the transverse strength of a magnetic field in an electrically conducting fluid increases the Lorentz force. This strength bears the potential to increase the blood temperature distribution.

Figure 10 shows that the velocity slip increases the temperature of the blood. The temperature distribution and the thermal boundary layer thickness increase with increasing slip for both the carrier-based fluid and the gold particle nanofluid because the slip slows down the fluid motion and ultimately affects the temperature. It is also evident from this figure that the increase in temperature is more for the nanofluid as compared to the regular fluid for the larger impacts of slip constraint.

Figure 11 shows that for larger values of suction, the blood temperature at any point of the flow is moderate for both the carrier-based fluid and the gold particle nanofluid. The thermal boundary layer thickness and the temperature distribution decrease at higher suction for both fluids. Stretching/shrinking reduces the temperature, as shown in Figure 12, for both fluids. A similar behavior is seen in Figure 12 for both fluids due to larger stretching compared to Figures 11 and 13, and shows that the temperature reduces due to the curvature for both fluids. The thermal boundary layer thickness and the temperature distribution decrease for both fluids due to the higher curvature. The figure insert shows the blood temperature distribution in terms of the significant effect of curvature, where the thermal conductivity is more for the gold particle nanofluid compared with the carrier-based fluid. From a physical point of view, this happens because the stretching curved surface increases the fluid flow for the velocity profiles and indirectly contributes to reducing the temperature distribution in terms of magnitude.

Radiation increases the temperature for both the carrier-based fluid and the gold particle nanofluid (Figure 14), which consequently increases the significant boundary layer thickness. Thus, the temperature of the boundary layer increases significantly. Moreover, the temperature distribution is greater for the gold particle nanofluid compared with the carrier-based fluid because the presence of gold nanoparticles produces more energy in the form of heat and, consequently, the temperature rises. The temperature increases due to the nanoparticle volume fraction in both fluids (Figure 15), because the inclusion of gold nanoparticles increases the thermal conductivity of blood, which increases the blood temperature.

### 3.3. Effect of Physical Parameters on the Skin Friction Coefficient and the Nusselt Number

The effects of the slip on skin friction coefficient and the Nusselt number against stretching/shrinking ( $\lambda$ ) for both the carrier-based fluid and the gold particle nanofluid are shown in Figures 16 and 17, respectively. The velocity slip enhances the skin friction coefficient but reduces the Nusselt number in both fluids. In addition, the skin friction coefficient significantly shrinks due to stretching/shrinking, whereas heat transfer increases. Moreover, the Nusselt number is higher in the gold particle nanofluid compared to the carrier-based fluid, which ultimately enhances thermal conductivity. The effects of suction on shear stress and heat transfer against  $\lambda$  are shown in Figures 18 and 19, respectively. The skin friction coefficient shrinks due to suction, whereas the Nusselt number increases. The thermophysical data of the base fluid (blood) and gold nanoparticles are listed in Table 1.

**Table 1.** Thermophysical properties of blood and gold nanoparticles (Koriko et al. [32]).

Thermophysical Properties	Blood	Gold
$\rho$ (kg/m <sup>3</sup> )	1050	19,300
$c_p$ (J/kgK)	3617	129
$\sigma$ (S/m)	1090	$4.1 \times 10^6$
$k$ (W/mK)	0.52	318

Finally, Table 2 presents a comparison of the current outcomes of the skin friction coefficient for  $B$  when  $B_1 = R_d = S = M = B_2 = \phi = 0$ ,  $\lambda = 1$ , and  $n = 1$ , which shows favorable agreement. For more details about the current technique, Table 3 shows a comparison of the current computational outcomes of the shear stress or friction factor for distinct values of the shrinking parameter when  $B \rightarrow \infty$ ,  $B_2 = M = \phi = B_1 = 0$ ,  $n = 1$ , and  $S = 2$  with the results of Roşca et al. [33]. The values show excellent agreement, proving the feasibility of the present numerical scheme. In addition, the numerical computational values of the skin friction coefficient and the heat transfer rate for the various constraints are given in Table 4 for both the carrier-based fluid ( $\phi = 0$ ) and the gold particle nanofluid ( $\phi = 0.035$ ), while the rest of the fixed parameters are  $Pr = 21$ ,  $n = 2$ ,  $S = 3.5$ , and  $B_2 = 0.2$ . For the carrier-based fluid, the skin friction coefficient increases by 18.815%, 27.626%, 6.231%, and  $1.552 \times 10^{-4}\%$  due to the impact of  $\lambda$ ,  $M$ ,  $B_1$ , and  $R_d$ , respectively, while it decreases by 1.774% due to  $B$ . By contrast, for the gold particle nanofluid, the skin friction coefficient increases by 18.311%, 15.034%, 4.541%, and  $3.207 \times 10^{-5}\%$  due to the effect of  $\lambda$ ,  $M$ ,  $B_1$ , and  $R_d$ , respectively, while it decreases by approximately 0.751% due to the curvature parameter. Moreover, due to  $\lambda$  and  $B_1$ , the heat transport rate increases by 0.157% and 0.031%, respectively, for the carrier-based fluid and by 0.156% and 0.027%, respectively, for the gold particle nanofluid. Due to the effect of the magnetic, curvature, and radiation parameters, the heat transport rate decreases by 0.078%,  $6.42 \times 10^{-3}\%$ , and 41.705%, respectively, for the carrier-based fluid and by 0.053%,  $8.39 \times 10^{-3}\%$ , and 41.045%, respectively, for the gold particle nanofluid. Generally, the increasing skin friction coefficient is better for both fluids due to the magnetic and stretching parameters, while it is lower (approximately  $1.552 \times 10^{-4}\%$  and  $3.207 \times 10^{-5}\%$ , respectively) for the radiation parameter. Alternatively, the heat transport rate is maximum for the stretching parameter for both fluids when the parameter increases and minimum (about  $6.42 \times 10^{-3}\%$  and  $8.39 \times 10^{-3}\%$ , respectively) for the curvature parameter. Finally, these numerically calculated values show that the skin friction coefficient and the heat transfer rate are largely found in the carrier-based fluid compared to the gold particle nanofluid.

**Table 2.** Comparison of the skin friction coefficient  $\left(-\frac{1}{2} Re_b^{\frac{1}{n+1}} C_F\right)$  for different values of  $B$  with the results of [34–36].

$B$	$-\frac{1}{2} Re_b^{\frac{1}{n+1}} C_F$			
	Saleh et al. [34]	Abbas et al. [35]	Waini et al. [36]	Current Outcome
5	1.15076	1.15763	1.15077	1.15756
10	1.07172	1.07349	1.07173	1.07347
20	1.03501	1.03561	1.03501	1.03566
30	1.02315	1.02353	1.02316	1.02353
40	1.01729	1.01759	1.01730	1.01704
50	1.01380	1.01405	1.01381	1.01440
100	1.00687	1.00704	1.00687	1.00703
200	1.00342	1.00356	1.00343	1.00354
1000	1.00068	1.00079	1.00068	1.00069

**Table 3.** Comparison of the skin friction coefficient  $\left(-\frac{1}{2}\text{Re}_b^{\frac{1}{n+1}}C_F\right)$  for different values of  $\lambda$  with the results of Roşca et al. [33].

$\lambda$	$-\frac{1}{2}\text{Re}_b^{\frac{1}{n+1}}C_F$		
	Roşca et al. [33]		Current Outcome
	Numerical Outcome	Analytical Outcome	
−0.5	0.85289	0.85355	0.85365
−0.6	0.9786	0.97947	0.97966
−0.7	1.08255	1.08340	1.08382
−0.75	1.12366	1.12500	1.12563
−0.8	1.15619	1.15777	1.15879
−0.9	1.18214	1.18460	1.18796
−0.95	1.15876	1.16242	1.16340
−0.99	1.08018	1.08900	1.09448

**Table 4.** Skin friction coefficient  $\left(\frac{1}{2}\right)\text{Re}_b^{\frac{1}{n+1}}C_F$  and Nusselt number  $\text{Re}_b^{\frac{-1}{n+1}}Nu_s$  for different parameters at  $\text{Pr} = 21$ ,  $n = 2$ ,  $S = 3.5$ , and  $B_2 = 0.2$ .

$\lambda$	$M$	$B$	$B_1$	$R_d$	$(1/2)\text{Re}_b^{\frac{1}{n+1}}C_F$		$\text{Re}_b^{\frac{-1}{n+1}}Nu_s$	
					$\phi=0$	$\phi=0.035$	$\phi=0$	$\phi=0.035$
1.5	0.5	1.5	0.3	2.0	5.92616	8.10476	27.00936	28.70528
1.7	-	-	-	-	7.04118	9.58888	27.05197	28.75033
1.9	-	-	-	-	8.23084	11.15728	27.09459	28.79556
1.5	0.5	1.5	0.3	2.0	5.92616	8.10476	27.00936	28.70528
-	5.0	-	-	-	7.56336	9.32326	26.98816	28.68989
-	10.0	-	-	-	8.74439	10.33223	26.97428	28.67789
1.5	0.5	1.5	0.3	2.0	5.92616	8.10476	27.00936	28.70528
-	-	2.0	-	-	5.82099	8.04389	27.00762	28.70287
-	-	2.5	-	-	5.76707	8.01154	27.00647	28.70138
1.5	0.5	1.5	0.3	2.0	5.92616	8.10476	27.00936	28.70528
-	-	-	0.7	-	6.29542	8.47280	27.01654	28.71433
-	-	-	1.1	-	6.70957	8.85348	27.02234	28.72237
1.5	0.5	1.5	0.3	2.0	5.92616	8.10476	27.00936	28.70528
-	-	-	-	4.0	5.92617	8.10476	15.74498	16.92315
-	-	-	-	6.0	5.92617	8.10476	11.14985	12.03202

#### 4. Conclusions

This study discussed the effects of a magnetic field on the flow of Sisko fluid containing gold nanoparticles over a porous, curved surface in the presence of radiation and partial slip. The key outcomes were as follows:

- The velocity of blood containing gold nanoparticles decreases with increasing intensity of an external magnetic field.
- The effect of thermal radiation can significantly modify the blood temperature. With increasing thermal radiation, the thickness of the thermal boundary layer increases significantly.
- An increase in the erythrocyte slip at the curved wall surface increases the temperature of the boundary layer.

- When suction increases in the curved wall surface, both the temperature and the velocity of blood decrease.

The current theoretical estimates will be significant for the more precise treatment of patients with regard to better outcomes of thermal therapy for reducing pain. In addition, this investigation will improve the understanding of thermal processes that occur during blood flow in arterial microvessels. Clinicians involved in tumor and cancer treatment will begin using the electromagnetic hyperthermia technique, which involves overheating target tissues to about 42 °C. The results show that the flow velocity of blood can be managed by suitably adjusting (decreasing/increasing) the magnetic field intensity. This finding should help surgeons who generally want to maintain blood flow at a preferred level throughout surgery.

**Author Contributions:** Conceptualization, A.Z. and A.I.; Formal analysis, A.Z. and A.I.; Methodology, U.K., A.Z. and A.I.; Software, U.K.; Supervision, A.Z. and A.I. All authors have read and agreed to the published version of the manuscript.

**Funding:** This research was funded by Universiti Kebangsaan Malaysia (project code: DIP-2020-001).

**Institutional Review Board Statement:** Not applicable.

**Informed Consent Statement:** Not applicable.

**Data Availability Statement:** Not applicable.

**Acknowledgments:** We gratefully acknowledge the financial support received from the Universiti Kebangsaan Malaysia (project code: DIP-2020-001).

**Conflicts of Interest:** The authors declare no conflict of interest

## References

- Choi, S.U.S.; Eastman, J.A. Enhancing thermal conductivity of fluids with nanoparticles. *ASME Fluids Eng. Div.* **1995**, *231*, 99–105.
- Eastman, J.A.; Choi, U.S.; Li, S.; Thompson, L.J.; Lee, S. Enhanced Thermal Conductivity through the Development of Nanofluids. *MRS Proc.* **1996**, *457*, 3–11. [[CrossRef](#)]
- Sheikholeslami, M.; Ganji, D.D.; Javed, M.Y.; Ellahi, R. Effect of thermal radiation on magnetohydrodynamics nanofluid flow and heat transfer by means of two-phase model. *J. Magn. Magn. Mater.* **2015**, *374*, 36–43. [[CrossRef](#)]
- Ellahi, R.; Hassan, M.; Zeeshan, A. Shape effects of nanosize particles in Cu–H<sub>2</sub>O nanofluid on entropy generation. *Int. J. Heat Mass Transf.* **2015**, *81*, 449–456. [[CrossRef](#)]
- Sadaf, H.; Nadeem, S. Influences of slip and Cu-blood nanofluid in a physiological study of cilia. *Comp. Meth. Prog. Biomed.* **2016**, *131*, 169–180. [[CrossRef](#)] [[PubMed](#)]
- Noreen, S.; Rashidi, M.; Qasim, M. Blood flow analysis with considering nanofluid effects in vertical channel. *Appl. Nanosci.* **2017**, *7*, 193–199. [[CrossRef](#)]
- Ardahaie, S.S.; Amiri, A.J.; Amouei, A.; Hosseinzadeh, K.; Ganji, D.D. Investigating the effect of adding nanoparticles to the blood flow in presence of magnetic field in a porous blood arterial. *Inform. Med. Unlocked* **2018**, *10*, 71–81. [[CrossRef](#)]
- Ellelmy, A.F.; Elgazery, N.S.; Ellahi, R. Blood flow of MHD non-Newtonian nanofluid with heat transfer and slip effects. *Int. J. Num. Meth. Heat Fluid Flow* **2020**, *30*, 4883–4908. [[CrossRef](#)]
- Kamal, F.; Zaimi, K.; Ishak, A.; Pop, I. Stability analysis of MHD stagnation-point flow towards a permeable stretching/shrinking sheet in a nanofluid with chemical reactions effect. *Sains Malays.* **2019**, *48*, 243–250. [[CrossRef](#)]
- Waini, I.; Ishak, A.; Groşan, T.; Pop, I. Mixed convection of a hybrid nanofluid flow along a vertical surface embedded in a porous medium. *Int. Commun. Heat Mass Transf.* **2020**, *114*, 104565. [[CrossRef](#)]
- Waini, I.; Ishak, A.; Pop, I. Hybrid nanofluid flow past a permeable moving thin needle. *Mathematics* **2020**, *8*, 612. [[CrossRef](#)]
- Waini, I.; Ishak, A.; Pop, I. Squeezed hybrid nanofluid flow over a permeable sensor surface. *Mathematics* **2020**, *8*, 898. [[CrossRef](#)]
- Huang, X.; El-Sayed, M.A. Gold nanoparticles: Optical properties and implementations in cancer diagnosis and photothermal therapy. *J. Adv. Res.* **2010**, *1*, 13–28. [[CrossRef](#)]
- Mekheimer, K.S.; Hasona, W.; Abo-Elkhair, R.; Zaher, A. Peristaltic blood flow with gold nanoparticles as a third grade nanofluid in catheter: Application of cancer therapy. *Phys. Lett. A* **2018**, *382*, 85–93. [[CrossRef](#)]
- Lowe, G.D.; Rumley, A. The relationship between blood viscosity and blood pressure in a random sample of the population aged 55 to 74 years. *Eur. Heart J.* **1993**, *597*, 14.
- Thurston, G.B.; Henderson, N.M. Effects of flow geometry on blood viscoelasticity. *Biorheology* **2006**, *43*, 729–746. [[PubMed](#)]
- Khan, M.; Shahzad, A. On boundary layer flow of a Sisko fluid over a stretching sheet. *Quaest. Math.* **2013**, *36*, 137.e51. [[CrossRef](#)]
- Munir, A.; Shahzad, A.; Khan, M. Convective flow of Sisko fluid over a bidirectional stretching surface. *PLoS ONE* **2015**, *1*, e0130342. [[CrossRef](#)] [[PubMed](#)]



19. Khan, M.; Ahmad, L.; Khan, W.A. Numerically framing the impact of radiation on magneto nanoparticles for 3D Sisko fluid flow. *J. Braz. Soc. Mech. Sci. Eng.* **2017**, *39*, 4475.e87. [[CrossRef](#)]
20. Eid, M.R.; Alsaedi, A.; Muhammad, T.; Hayat, T. Comprehensive analysis of heat transfer of gold-blood nanofluid (Sisko-model) with thermal radiation. *Results Phys.* **2017**, *7*, 4388–4393. [[CrossRef](#)]
21. Ahmad, L.; Khan, M. Numerical simulation for MHD flow of Sisko nanofluid over a moving curved surface: A revised model. *Microsyst. Technol.* **2019**, *25*, 2411–2428. [[CrossRef](#)]
22. Khan, U.; Zaib, A.; Shah, Z.; Baleanu, D.; Sherif El-Sayed, M. Impact of magnetic field on boundary-layer flow of Sisko liquid comprising nanomaterials migration through radially shrinking/stretching surface with zero mass flux. *J. Mater. Res. Technol.* **2020**, *9*, 3699–3709. [[CrossRef](#)]
23. Inoue, S.; Kobaya, M. Biological activities caused by far infrared radiation. *Int. J. Biometeorol.* **1989**, *33*, 145–150. [[CrossRef](#)]
24. Kobu, Y. Effects of infrared radiation on intraosseous blood flow and oxygen tension in rat tibia. *Kobe J. Med. Sci.* **1999**, *45*, 27–39. [[PubMed](#)]
25. Nishimoto, C.; Ishiura, Y.; Kuniasu, K.; Koga, T. Effects of ultrasonic radiation on cutaneous blood flow in the paw of decerebrated rats. *Kawasaki J. Med. Welfare* **2006**, *12*, 13–18.
26. He, Y.; Shirazaki, M.; Liu, H.; Himeno, R.; Sun, R. A numerical coupling model to analyze the blood flow, temperature, and oxygen transport in human breast tumor under laser irradiation. *Comput. Biol. Med.* **2006**, *36*, 1336–1350. [[CrossRef](#)]
27. Prakash, J.; Makinde, O.D. Radiative heat transfer to blood flow through a stenotic artery in the presence of magnetic field. *Lat. Am. Appl. Res.* **2011**, *41*, 273–277.
28. Misra, J.C.; Sinha, A. Effect of thermal radiation on MHD flow of blood and heat transfer in a permeable capillary in stretching motion. *Heat Mass Transf.* **2013**, *49*, 617–628. [[CrossRef](#)]
29. Khan, U.; Shafiq, A.; Zaib, A.; Sherif El-Sayed, M.; Baleanu, D. MHD radiative blood flow embracing gold particles via a slippery sheet through an erratic heat sink/source. *Mathematics* **2020**, *8*, 1597. [[CrossRef](#)]
30. Zaib, A.; Khan, U.; Wakif, A.; Zaydan, M. Numerical entropic analysis of mixed MHD convective flows from a non-isothermal vertical flat plate for radiative tangent hyperbolic blood biofluids conveying magnetite ferroparticles: Dual similarity solutions. *Arabian J. Sci. Eng.* **2020**, *45*, 5311–5330. [[CrossRef](#)]
31. Chen, I.H. Analysis of an intensive magnetic field on blood flow: Part 2. *J. Bioelectr.* **1985**, *4*, 55–61. [[CrossRef](#)]
32. Koriko, O.K.; Animasaun, I.; Mahanthesh, B.; Saleem, S.; Sarojamma, G.; Sivaraj, R. Heat transfer in the flow of blood-gold Carreau nanofluid induced by partial slip and buoyancy. *Heat Transf. Asian Res.* **2018**, *47*, 806–823. [[CrossRef](#)]
33. Roşca, N.C.; Pop, I. Unsteady boundary layer flow over a permeable curved stretching/shrinking surface. *Eur. J. Mech. B/Fluids* **2015**, *51*, 61–67. [[CrossRef](#)]
34. Saleh, S.H.M.; Arifin, N.M.; Nazar, R.; Pop, I. Unsteady micropolar fluid over a permeable curved stretching shrinking surface. *Math. Prob. Eng.* **2017**, *2017*, 3085249. [[CrossRef](#)]
35. Abbas, Z.; Naveed, M.; Sajid, M. Heat transfer analysis for stretching flow over a curved surface with magnetic field. *J. Eng. Thermophys.* **2013**, *22*, 337–345. [[CrossRef](#)]
36. Waini, I.; Ishak, A.; Pop, I. Flow and heat transfer along a permeable stretching/shrinking curved surface in a hybrid nanofluid. *Phys. Scr.* **2019**, *94*, 105219. [[CrossRef](#)]